Ocean Engineering 270 (2023) 113535

Contents lists available at ScienceDirect

Ocean Engineering

journal homepage: www.elsevier.com/locate/oceaneng

A general framework to obtain seamless seasonal–directional extreme individual wave heights—Showcase Ekofisk

Patrik Bohlinger [a,*], Theodoros Economou [b], Ole Johan Aarnes [a], Mika Malila [a], Øyvind Breivik [a,c]

[a] Norwegian Meteorological Institute, Bergen, Norway
[b] The Cyprus Institute, Nicosia, Cyprus
[c] Geophysical Institute, University of Bergen, Bergen, Norway

ARTICLE INFO

Keywords:
Extreme wave heights
Generalized additive models
von Mises distribution
Seasonal–directional extremes
Covariates

ABSTRACT

Extreme wave climate provides the basis for safe design of offshore structures and is crucial for planning and executing offshore operations. Covariate modeling of extremes significantly enriches and improves estimates of return levels and exceedance probabilities of extreme sea states. Based on novel observational and hindcast datasets, we formulate a seasonal–directional extreme value model for individual wave heights and present exceedance probabilities for the Ekofisk oil and gas field, a location in the Central North Sea. Subsequently, we elucidate how to downscale estimates of monthly exceedance probabilities and return levels to daily maxima and illustrate how to retrieve consistent results on seamless directional sectors and different seasons, or for the entire covariate space. We conclude with a versatile statistical framework to obtain seasonal–directional extreme waves and reveal a strong seasonal and directional dependence of extreme individual waves at Ekofisk with the highest waves coming from northwest during winter. Moreover, we apply our approach to normalized wave heights and show noticeable variability depending on season and direction with implications for offshore design.

Sea state conditions in the North Sea expressed by the parameter significant wave height (H_s) depict directional and seasonal dependencies (Feld et al., 2014, 2019; Hansen et al., 2020) and the probabilities of the occurrence of extreme sea states can vary dramatically. In order to correctly estimate exceedance probabilities, it is crucial to take non-stationarity into account (Jonathan et al., 2008; Jonathan and Ewans, 2011, 2013). Recent studies (Breivik et al., 2022; Malila et al., 2022b,a) provide a data base that allows us to apply this knowledge to observed individual waves. In what follows, we present a statistical framework on how to retrieve seamlessly customizable seasonal–directional extreme individual wave heights.

A convenient, and therefore common, approach to statistically model non-stationary extreme values is to condition parameters of the extreme value model on variables that are the suspected cause of non-stationarity. The nature of the dependency is not necessarily linear and is often unknown. A way of dealing with unknown but assumed smooth dependencies in a model with covariates, is to utilize regression splines as incorporated in a Generalized Additive Model (GAM) (Wood, 2017) where dependence on cyclic variables can elegantly be implemented using cyclic splines.

Interestingly and importantly, it can be crucial to take into account non-stationary behavior even if one only plans to use stationary exceedance probabilities. Jonathan et al. (2008) demonstrated that omni-directional estimates from a stationary model resulted in heavily biased estimation of return values while omni-directional estimates from a directional model were almost unbiased. For the North Sea, H_s extremes from the NORA10 wave hindcast (Reistad et al., 2011) were shown to depend on both season and direction (Jonathan et al., 2008; Feld et al., 2014). Similar to H_s, we also expect individual waves to display directional and seasonal dependency.

The typical prime source of sea surface elevation observations for studying individual waves are offshore platforms. There are few publicly available time series which, however, encompass a large amount of data across many platforms world wide (Christou and Ewans, 2014; Häfner et al., 2021). In recent years, Gaussian process (GP) models have proven to be useful for filtering wave related time series (Bohlinger et al., 2019; Malila et al., 2022b). This finally resulted in a unique, high-quality dataset (Malila et al., 2022a) tailored to the analysis of extreme waves where the existence of four simultaneous measuring lasers help to determine whether an observation is a true measurement or should be discarded. We base our study on this novel dataset that focuses on preserving the extremes.

* Corresponding author.
E-mail address: patrikb@met.no (P. Bohlinger).

https://doi.org/10.1016/j.oceaneng.2022.113535
Received 12 October 2022; Received in revised form 8 December 2022; Accepted 22 December 2022
Available online 10 January 2023

Fig. 1. Left: Ekofisk location in the central North Sea marked by the red dot. Center: Footbridge between the Ekofisk 2/4 K and 2/4 B platforms, looking toward the 2/4 B platform. Right: The 4 laser altimeters placed in a 2.6 m × 2.6 m array formation inside the footbridge.

Combining direct sea surface elevation measurements with wave direction from the novel wave model hindcast NORA3 (Breivik et al., 2022), we develop a seasonal–directional extreme value model to estimate exceedance probabilities of monthly maxima for a location in the central North Sea, the Ekofisk oil and gas field. To contextualize our results, we will showcase exceedance probabilities for extreme wave heights with magnitudes comparable to the famous Andrea freak wave (Donelan and Magnusson, 2017). Moreover, we demonstrate how this model can be used to up- or downscale the results in the covariate space according to user needs.

We start by first describing our data basis and the methodology, including details about the statistical model. We continue with general results from the model, aggregation across the covariate space, and tailoring the results to user needs. Finally, we provide our thoughts on the limitations of this model together with a conclusion and an outlook addressing possible future extensions.

1. Data description and related challenges

The observational data base for our study comes from a laser array mounted on the Ekofisk oil and gas field located in the central North Sea (Fig. 1). The laser array consists of four Optech Sentinel 3100 infrared laser altimeters that measure the distance to the sea surface at a frequency of $f_{LA} = 5$ Hz. The dataset was originally noisy mainly due to sea spray and specular reflection occurring especially during calm sea states, and contained missing values due to random system failures and subsequent maintenance periods. For the purpose of exploring extreme waves this dataset has been filtered utilizing a GP model (Malila et al., 2022b) and was made publicly available for further studies (see Malila et al., 2022a). For our study we will use the up-crossing wave height (H_U) time series of the highest available quality level (QC3).

To avoid counting the same wave multiple times we merged the time series of the four lasers by choosing for each time step the value from the preferred laser. The order of preference is L_2 (best), L_1, L_3, and L_4 (worst). The order was determined from the experienced quality of the lasers during data acquisition and preparation of Malila et al. (2022b,a). The resulting merged time series encompasses the years 2003–2020. For details on the filtering method and the dataset please refer to Malila et al. (2022b,a), respectively.

The H_U time series consists of 9,213,028 waves after the quality control procedure. A pronounced seasonal cycle is visible with the lowest H_U values recorded in summer and the highest during the storm season in fall and winter (Fig. 2). This causes clusters and auto-correlation that need to be taken into account when computing exceedance probabilities. For the North Sea, Bell et al. (2017) found that prevailing northerly winds have the greatest potential for building the highest sea states. It is thus already known that there is a directional dependency for high sea states in the North Sea and directional information needs to be considered. Since storms, that occur mainly in the storm season, will preferably cause large waves from specific directions due to the effective fetch length and low pressure tracks, it is reasonable to assume that season and direction are not completely independent which should be dealt with adequately.

Another challenge are missing data due to instrument or software failures, and erroneous observations that lead to censoring. Although the instrument can randomly fail, there is a type of systematic left censoring due to the physical measurement principle of the laser. Whenever the sea is too calm/flat, specular reflection can occur and yield missing/erroneous recordings (Malila et al., 2022b). This occurs mainly during low sea states below H_s of roughly 3 m and consequently during the summer months. If no informative insights exist on the censoring mechanism, a zero-order approach would be to consider waves for given sea states, typically done by calculating the normalized wave heights $H_{norm} = \frac{H_U}{H_s}$. For these ratios, there exist physically reasoned and mathematically derived equations, i.e., the theoretical Rayleigh (Rayleigh, 1880) and Tayfun (Tayfun, 1980) distributions, expressing their probability of exceedance. The downside is that these theoretical distributions are merely a reference, do not incorporate all possible physical processes, and therefore might not correctly describe all waves at the site of interest. Another disadvantage when working with H_{norm} while interested in the exceedance probability of an individual wave is that the sea state needs to be known. When in addition there is interest in the exceedance probability given a direction and/or season, there is little variability left to be explained by this information as H_s already explains most of the variability of H_U given their above mentioned physical relationship (Fig. 4 right). In fact, for this feature to change in a given direction and season, the presence of some physical mechanism is required to alter these ratios systematically. Although this can certainly be of interest, in this paper we focus on extreme absolute heights of individual waves and thus cannot avoid the censoring challenge by choosing H_{norm}. We will, however, briefly show an application to normalized wave heights.

2. Methodology

2.1. Strategy to meet the challenges

As already described, the laser dataset poses multiple challenges. In short those consist of (1) auto-correlation, (2) systematic censoring, (3) cyclic variables as covariates, (4) directionality is needed but not present in the laser data, and (5) correlated covariates. We propose the following strategies to handle these challenges.

(1) and (2): By choosing monthly maxima we avoid most of the problematic censoring. Considering a threshold approach or higher temporal resolution approach will need to be followed with a statement about the likelihood of exceedance of the threshold when part of the data is not known. Daily maxima bring about the problem with days that come without any data because of calm sea conditions, which consequently leads to a systematic under-representation of low daily maxima. When considering monthly maxima, however, it is less likely that entire months are censored due to calm seas and that the monthly

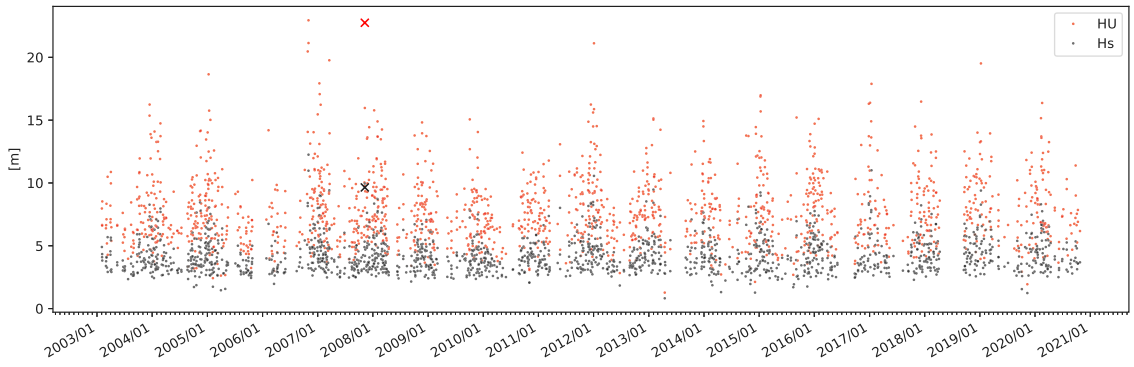

Fig. 2. Time series of hourly maxima of H_U and H_s from combined time series. The crosses denote the recording of the Andrea freak wave.

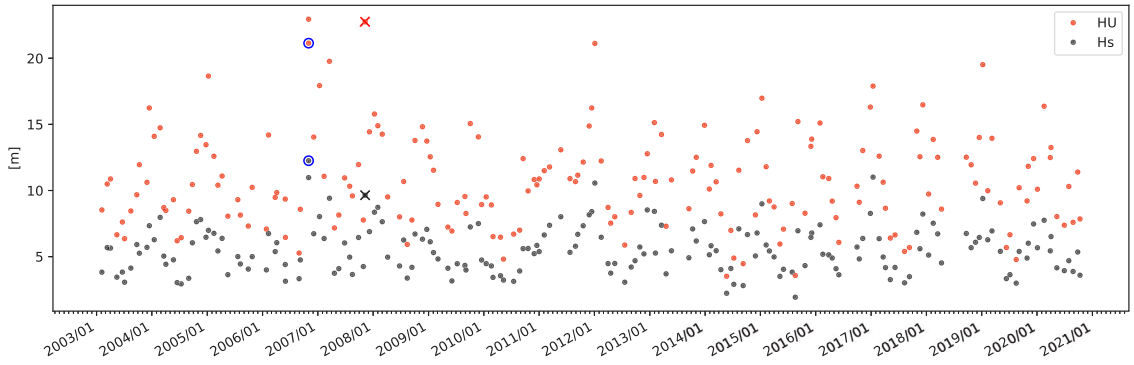

Fig. 3. Time series of monthly maxima of H_U and H_s from combined time series. The crosses denote the recording of the Andrea freak wave. The blue circles mark the maximum that was removed due to correlation.

maxima are suspect to systematic left censoring. In fact, the retained maxima are consequently likely real monthly maxima as all other waves were in too low sea states to be measured. Considering monthly maxima also mitigates the issue of auto-correlation as it is unlikely that a storm crosses the boundaries between months and creates monthly maxima related to the same storm. There is, however, one exception which we removed (Fig. 3). In this case, two maxima occurred only a few hours apart and were created by the same storm system.

(3): We use both directionality (0–360°) and seasonality (months 1–12), as covariates for our extreme value model. Both covariates are cyclic and need to be dealt with appropriately. Therefore, we model the dependency of the model parameters on these covariates utilizing penalized cyclic cubic regression splines.

(4): As has been shown in previous studies, directionality should be included and is also demanded by users. We have not yet found a reliable way to systematically retrieve directions from the laser array and use therefore the novel NORA3 hindcast dataset (Breivik et al., 2022) to retrieve the direction of the dominant sea partition called peak direction (PDIR) as a proxy for wave direction.

(5): We will deal with correlation between covariates, i.e., dependency between direction and month of year, using tensor product smoothers (Wood, 2006, 2017). The use of these smoothers is appropriate when dealing with multiple covariates of completely different magnitude and when non-isotropic behavior is assumed.

The basis for our statistical model are the monthly maxima of the original dataset which reduces to 191 values across 18 years (2003–2020) (Fig. 3) with a clear dependency on season and direction (Fig. 4, left and center). The highest sea states and individual waves occur in storms during the fall and winter seasons with waves approaching Ekofisk from the northwest.

2.2. Clarification on the term "exceedance probability"

It is important to distinguish between different exceedance probabilities that may at first glance seem similar but really are not the same and can take fundamentally different values. For this study, we are interested in an exceedance probability given a threshold, a direction, and the season. For clarification of the results there are the following probabilities to consider:

- In a situation where waves come from a certain direction during a certain season one might wonder what is the probability, given these conditions, that a wave will exceed a critical threshold. The answer to that question would be what we coin here the *conditional probability* (CP).
- Another important probability is the *occurrence probability* (OP) of the respective conditions, since we are interested in a probability varying with season and direction.
- Finally, we define the *total probability* (TP) which combines CP and OP and can thus more generally answer the question on how likely it is that a wave exceeds a threshold from a direction during a given season while incorporating the fact that the conditions are only a subset of what can occur, be it seldom or frequent. For offshore design, TP is typically most important as it indirectly dictates the loads an offshore structure has to withstand and in this form TP is comparable with the non-stationary, and hence omni-directional, exceedance probability.

When considering directions, the probability for one wave to be large from a direction with high probability of large waves is of course higher than for a direction with low probability of large waves. When allowing for a wave to come from a random direction, the probability for this wave to be large is somewhere in the middle because there is a chance that a direction with a low or high probability for large waves are chosen. This probability is of type CP, i.e., without considering the effect of OP. Although this could technically be called omni-directional, as one allows the wave to come from any direction, this is not what is typically meant in offshore standards. When demanding that omni-directional extremes have to be larger than extremes from the direction

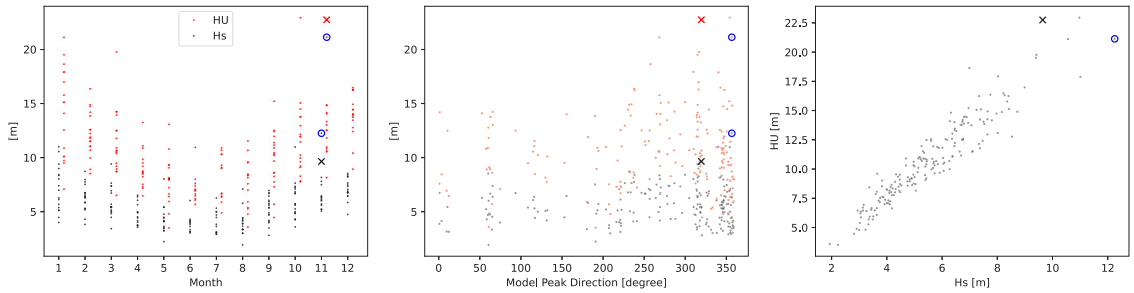

Fig. 4. Diagnostic figures visualizing the data basis consisting of monthly maxima. The crosses denote the recording of the Andrea freak wave. The blue circles mark the maximum that was removed due to correlation.

with the highest probability for large waves, the NORSOK standard operates with extremes and their probabilities of type TP.

The same is true when, instead of directions, one considers seasons or months of the year versus omni-seasonal extremes. Even though extreme waves in January are among the largest during a year, it is more likely a wave exceeds a threshold when allowing for more time to pass, i.e., the aggregated probability over multiple months or seasons. So instead of denoting extremes and their probability from a random month (CP) omni-seasonal, omni-seasonal typically means the aggregation of all months (TP) which then considers also OP.

Finally, the choice of months and directions can be combined arbitrarily. For the discussion of our results we make the following distinctions:

- An omni-seasonal and omni-directional model aggregated along neither dimension would just be denoted *omni-directional/seasonal CP*.
- An omni-seasonal and omni-directional model aggregated along both dimensions would just be denoted *omni-directional/seasonal TP*.
- If one dimension is not aggregated it will be explicitly added to the name, e.g.: *omni-directional TP for January* or *omni-seasonal TP for* {NameOfSector}. The same applies for combinations with CP.

2.3. Model description

We use extreme value theory (Coles, 2001) and apply a Generalized Extreme Value (GEV) distribution whose parameters are expressed as smooth functions of month and direction. This is implemented as a Generalized Additive Model or GAM (Wood, 2017), using the R package `mgcv`. In GAMs, smooth functions of covariates use penalized regression splines, so a smooth function of covariate x_i say, is constructed as a linear combination

$$f(x_i) = \sum_{k=1}^{K} \beta_k b_k(x_i) = \boldsymbol{X}_i \boldsymbol{\beta} \tag{1}$$

where $\boldsymbol{\beta} = \{\beta_k\}$ are unknown coefficients ($k = 1$ conventionally aliased to an intercept) and $b_k(\cdot)$ are basis functions such as cubic splines. Matrix $\boldsymbol{X}_i = \{b_k(x_i)\}$ with dimension $n \times K$ (n being the number of data points) is the model matrix. The value of K (known as the number of knots) determines the flexibility of $f(\cdot)$. The model is estimated using penalized likelihood, where the penalty restricts the amount of flexibility in $f(\cdot)$ in order to avoid overfitting (Wood, 2011). Specifically, the log-likelihood to be maximized is written as

$$\ell(\boldsymbol{\beta}, \theta; \boldsymbol{y}) - \lambda_\beta \boldsymbol{\beta}' \boldsymbol{S}_\beta \boldsymbol{\beta} \tag{2}$$

where $\ell(\cdot)$ is the log-likelihood, θ are other model parameters and λ_β is a penalty parameter. The penalty matrix $\boldsymbol{S}_\beta$ relates to a quadratic penalty on $\boldsymbol{\beta}$. The second term in (2) penalizes the flexibility (wiggliness) of $f(\cdot)$ so that the larger λ_β is the more the penalization.

The fact that in GAMs we assume a priori that all unknown functions of the covariates are smooth can be viewed as a constraint on the values that $\boldsymbol{\beta}$ can take. From a Bayesian viewpoint, this can be achieved by assuming that $\boldsymbol{\beta}$ has the following prior distribution:

$$\boldsymbol{\beta} \sim N(\boldsymbol{0}, \boldsymbol{S}^- / \lambda_\beta) \tag{3}$$

where $\boldsymbol{S}^-$ is the pseudo-inverse of the penalty matrix $\boldsymbol{S}$ (Wood, 2017). The posterior distribution can be approximated by a multivariate Normal and is readily provided after fitting the model in the R package `mgcv`. Using this, we can then obtain samples from the posterior predictive distribution of H_U for any value of direction or month, this being a distribution that includes all associated uncertainty (Gelman et al., 2013).

Lastly, functions of more than one covariate can be constructed using tensor product interactions (Wood, 2017) where a smooth function of x_i and z_i say, can be constructed by making the coefficients of Eq. (1) smooth functions of z, e.g.

$$f(x_i, z_i) = \sum_{j=1}^{J} \beta_j(z_i) b_j(x_i) \tag{4}$$

where $\beta_j(z_i) = \sum_{m=1}^{M} \gamma_{j,m} a_m(z_i)$ and where $a_m(\cdot)$ can be of different basis than $b_j(\cdot)$.

2.4. Model specification

We fit the following model for y_m being maximum H_U at month m:

$$y_m \sim \mathrm{GEV}(\mu_m, \sigma_m, \xi) \tag{5}$$

$$\mu_m \sim f(m, d(m)) \tag{6}$$

$$\log(\sigma_m) \sim g(m, d(m)) \tag{7}$$

where μ_m, σ_m and ξ are the location, scale and shape parameters of the GEV. Smooth functions $f(\cdot)$ and $g(\cdot)$ are tensor products of month m and direction $d(m)$. These are constructed using a cyclic cubic spline for each covariate and then interacted as in Eq. (4). Cyclic splines have an added constraint that the smooth functions join at the end points (e.g., month 1 and 12, and angle 0° and 360°). We choose 63 knots for each of the two functions (which was judged adequate using `mgcv`'s function `gam.check`). The shape parameter (median ca. −0.11,) was left constant since introducing non-stationarity did not improve our model.

2.5. Model predictions and checking

Fitting the model in `mgcv` and obtaining samples from the posterior predictive distribution of the observed H_U values allows for thorough model checking. In practice, this involves simulation from the posterior distribution of the spline coefficients Eq. (3), and then for each such sample a further simulation from the GEV distribution.

We assess the quality of our model by checking whether samples from the posterior predictive distribution resemble the empirical distribution of the observations. Our model tends to slightly underpredict the highest waves compared to the empirical distribution of

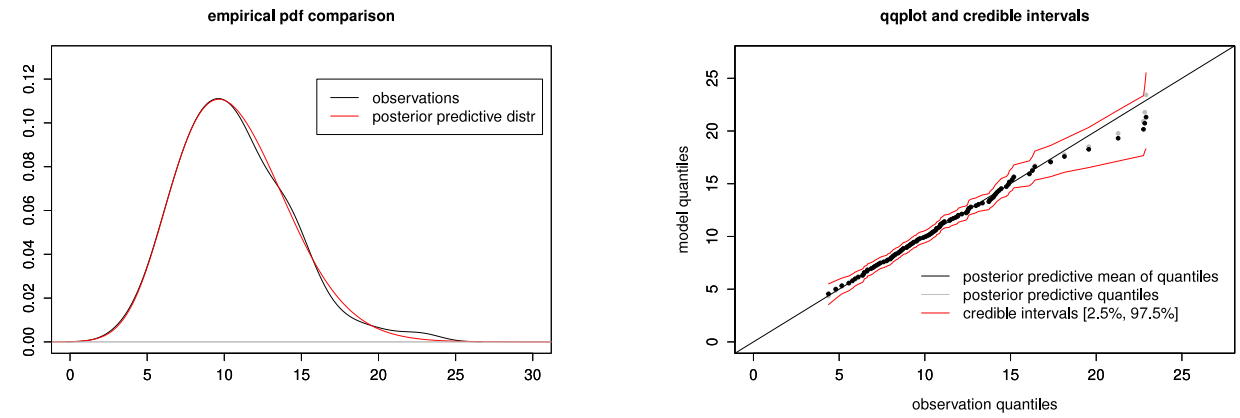

Fig. 5. Validation of our statistical model. Left: comparison of the empirical pdf from the observations against the model pdf from the posterior predictive distribution. Densities are estimated with a Gaussian kernel smoother of width 5 both for model and observation distributions. Right: A QQ-plot comparing the mean of 1000 simulated values for each observation (black) with 2.5% and 97.5% quantiles as credible intervals (red) and quantiles from all simulated data (gray) against the quantiles from the observations.

the observations (Fig. 5, left). However, the slight wiggly behavior of the observation quantiles may be caused by the limited number of considered observations. This becomes more clear when comparing the distributions in a QQ-plot (Fig. 5, right). Although the highest quantiles of the simulated maxima are lower than the highest quantiles of the observed maxima, the observations still lie well within the prediction intervals of the simulated maxima, meaning our model allows for higher maxima to occur.

We tested also a non-stationary shape parameter incorporating direction and season comparing the Akaike Information Criterion (AIC) which is defined as

$$\mathrm{AIC} = 2k - 2\ln(\max(\mathcal{L})) \tag{8}$$

with the likelihood function $\mathcal{L}$ and the number of estimated parameters k. Including the number of estimated parameters the AIC penalizes for model complexity and discourages overfitting. However, we obtained almost identical results (not shown) with a non-stationary shape parameter. Since the AIC was slightly higher (stationary shape: AIC = 886, 63 knots for location and scale, respectively; non-stationary shape: AIC = 894, 48 knots for location, scale, and shape, respectively), indicating no additional benefit for the increased complexity, we choose the simpler model and continue with a stationary shape parameter.

2.6. Stationary baseline model

For comparison with our non-stationary GAM, we fit a stationary GEV distribution using the extRemes package (Gilleland and Katz, 2016) with the default maximum likelihood estimation method. As data base we had to choose annual maxima instead of monthly maxima to satisfy the constraint that all values must be independent and identically distributed (i.i.d.) random variables. The resulting GEV distribution has a slightly negative shape parameter close to zero and is almost Gumbel type with parameters $\mu = 15.72$, $\sigma = 2.27$, and $\xi = -0.01$.

3. Results

The estimated location and scale parameters exhibit a clear seasonal and directional dependency (Fig. A.11) and vary considerably across the covariate space. The shape parameter indicates a GEV of type III but allows also for predictions from a long-tailed, Fréchet-type GEV (Fig. A.12). The landscapes of location and scale leave their imprints on the exceedance probability landscapes (Fig. 6).

We compute exceedance probabilities for monthly maxima of individual waves larger than 12 m (Fig. 6 left) and 21 m (Fig. 6 right). The first threshold of 12 m is a common threshold of interest for Ekofisk and 21 m is about the size of the famous Andrea wave. The largest waves and the highest probabilities for exceeding the thresholds are in the fall and winter season. 12 m is being exceeded virtually every year consistent with the time series of monthly maxima (Fig. 3). During summer the sea states in the central North Sea are much more calm and large waves are very unlikely. An Andrea type wave exceeding a threshold of 21 m seems only possible in winter and from north or northwest. Then, however, during the winter months the chance of exceeding a 21 m wave height can be as high as CP = 0.033. From the south and east and especially in summer it is virtually impossible to build up sea states that can lead to such large waves. This result is consistent with the fetch length available for building up phenomenal sea states and Bell et al. (2017) who state that northerly winds are most likely to create high sea states in the North Sea.

4. Accounting for user needs

The following section describes how we would apply our model to tasks frequently required by the offshore sector. We delineate three showcases that should enable the reader to perform methodological extrapolation to other similar cases.

4.1. Downscaling return levels and probabilities: From monthly to daily estimates

As explained in the beginning, we were using monthly maxima to construct the statistical model. However, when planning offshore operations, considering monthly block maxima might be too coarse. In this case, the return levels and exceeding probabilities can be adjusted and downscaled to, e.g., daily estimates. Assuming that, just like the monthly maxima, the daily maxima are independent one could compare the probabilities,

$$P\left(X_{\mathrm{m}} \leq T\right) = \left[P\left(X_{\mathrm{d},m} \leq T\right)\right]^{n} \tag{9}$$

where X_{m} are the monthly maxima, X_{d} represent the daily maxima within the month m, T some threshold, and n is the number of considered days in a month m. In terms of GEV distribution function, downscaling with the power of n becomes

$$G(z)^{n} = \left(\exp\left\{-\left[1+\xi_m\left(\frac{z-\mu_m}{\sigma_m}\right)\right]^{-\frac{1}{\xi_m}}\right\}\right)^{n} \tag{10}$$

where G is the GEV distribution function with shape parameter ξ, location μ, and scale σ. In this way, the probability can be scaled to some multiple of n corresponding to, e.g., one day or to an arbitrary time window of operation. Estimates of extreme quantiles of the daily

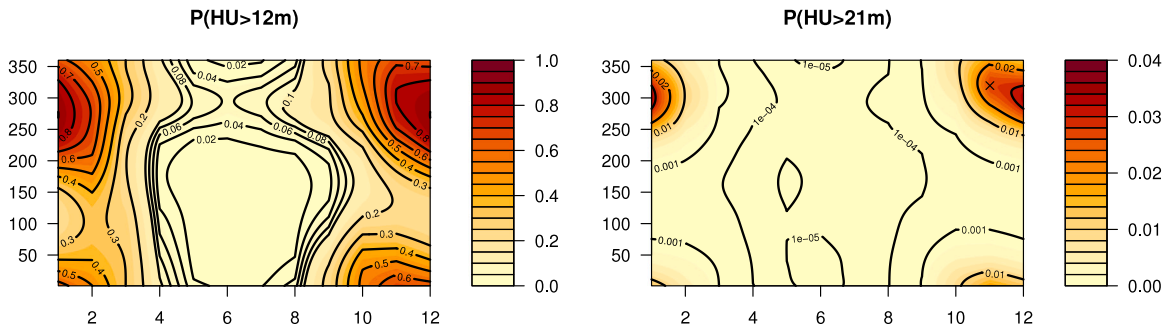

Fig. 6. Exceedance probability landscape (CP) for given wave direction (coming from) and month for the exceedance of two different thresholds 12 m (left) and an Andrea type wave of 21 m (right). The position of the Andrea wave on the landscape figure is marked with a black cross. Note the different color scales for each panel.

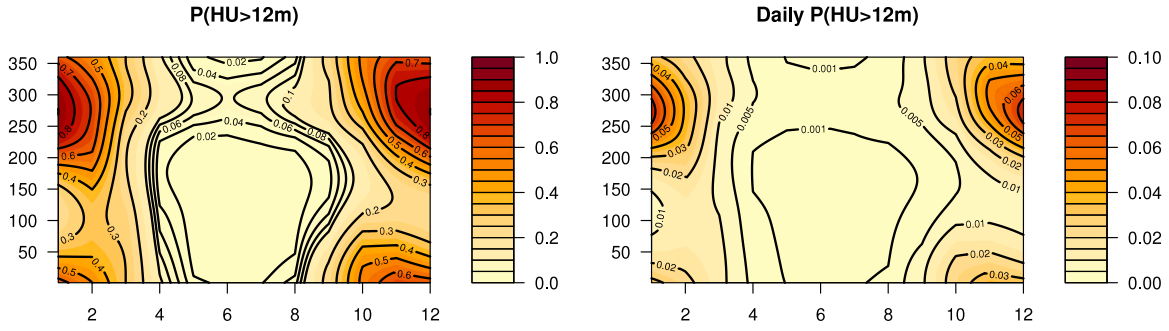

Fig. 7. Exceedance probability landscapes (CP) for an individual wave higher than a threshold of 12 m. Left: same as in Fig. 6 (left). Right: Exceedance probability for a given direction and day in a given month. Note the different color scales for each panel.

maxima distribution for a given month can then be obtained for $\xi \neq 0$ as

$$z_p = \mu_m - \frac{\sigma_m}{\xi_m}\left[1 - \{-n \log(1-P)\}\right] \tag{11}$$

with the probability P, the considered month m, and number of days in the month n which can be chosen freely.

This results in an exceedance probability landscape (Fig. 7) similar to the monthly maxima but with the lower probabilities corresponding to the duration of one day. When interested in specific time windows this approach can easily be adjusted even if transitioning between months.

Although we used daily maxima in this example, it is important to note that this is for illustration purposes. If wave maxima are assumed to be correlated, for instance due to a decorrelation time scale within storms longer than a day, then the time period needs to be prolonged.

4.2. Results tailored to directional sectors and arbitrary subsets of the covariate space

Commonly an offshore operator needs to consider a directional sector rather than one specific direction. One key question is whether the directions within the chosen sector can be considered approximately equally likely to occur or not. If the directions are equally likely to occur one can assume a uniform distribution and establish a fine grid to approximate sampling along the continuous spline in our GAM GEV model.

If, however, as in our case, the occurrence probabilities of directions vary with season, we model first the directions for each month using a cyclic statistical model, i.e., the von Mises distribution (von Mises, 1918) included in the R package `circular` (Agostinelli and Lund, 2022). We then sample directions from the cyclic model valid for the sector of interest to subsequently exploit the Bayesian interpretation of our spline-based non-stationary GAM GEV model and sample from the posterior predictive distribution monthly maxima for the directions of the chosen sector and month. Finally, we set a threshold T and count exceedances of all return levels and compute the exceedance probability ($\mathrm{CP} = P(X_m > T|s,m)$) for the desired sector and month.

As already mentioned, an offshore operator might want to combine CP with OP of sea from a given sector and month. OP is equal to the fraction of directions from our monthly von Mises model within a sector divided by all sampled directions. The larger the sector the larger the probability and for the omni-directional case this converges to 1 while narrow sectors will be scaled with a fraction of 1 accordingly. It is now straightforward to formulate and compute the total exceedance probability TP,

$$\mathrm{TP}(X > T|s,m) = \mathrm{OP}(s,m) \cdot \mathrm{CP}(X > T|s,m) \tag{12}$$

As thoroughly illustrated by Feld et al. (2019), the common approach to account for OP in directional probabilities or return levels is to artificially re-scale either one or the other in cases where directional estimates exceed omni-directional estimates (omni-directional TP). This is inconsistent as it is not applied always, the re-scaling is done in the aftermath, the re-scaled estimates may lead to a mismatch in return periods, and as Feld et al. (2019) points out, the approach is not clearly defined in the offshore standards. Using the approach we describe, one does not need any re-scaling or adjustment of this kind, once the results are retrieved. The retrieval of the results is by definition consistent and any prediction from an arbitrary sector or time period can directly be put in context to an omni-seasonal or/and omni-directional estimate. Predictions are consistent when moving from a point estimate, represented by a very narrow sector, to a directional sector or seasonal estimate and further to omni-directional and omni-seasonal predictions. As commonly required by offshore design and operation guidelines, e.g., NORSOKSTANDARD N-003 (2017), and summarized for directional estimates by Feld et al. (2019), predictions for the sector most prone to extremes can thus never exceed omni-directional/seasonal predictions because they are scaled by OP for the given sector and the temporal range. This can be done seamlessly along the covariate space without pre-defining e.g. sectors prior to a model fit.

Table 1
Exceedance probabilities for monthly maxima from various sector/month combinations as well as the respective omni-directional probabilities. Probabilities are computed for a threshold of 12 m and 21 m based on 1000 model predictions for each considered scenario.

	January OD	January S1	January S2	July OD	July S1	July S2
$P(H_U > 12\ m)$	0.846	0.136	0.007	0.037	0.016	0.000
$P(H_U > 21\ m)$	0.031	0.005	0.000	0.000	0.000	0.000

4.3. Practical showcase illustration

To illustrate the consistency of our approach, we compute exceedance probabilities for two directional sectors and two different months as well as for the omni-directional and omni-seasonal case. Fig. 8 (left) shows directions from all observed monthly maxima spread across the directional circle with the majority of cases coming from the northwest. The occurrence probability of directions for monthly maxima varies with season which is illustrated by von Mises densities for January and July (Fig. 8 center and right). We consider the directional sectors S1 comprising 300° to 330° (depicted in orange) and S2 for 120° to 150° (in cyan). Those sectors are chosen because S1 resembles a region on the directional dimension with a high probability to encounter large waves and S2 represents the counterpart with a low probability of experiencing large waves, varying slightly with season (Fig. 6).

Table 1 summarizes the omni-directional and sectorial probabilities for January and July. Note that, as demanded by the previously mentioned guidelines like NORSOK, TP from the most exposed sector S1 is less than for the omni-directional case without applying artificial scaling. In January it is almost 85% certain that a wave larger than 12 m will pass under the laser altimeter. Waves larger than 21 m still have a 3% chance to occur. When only allowing waves from S1 the chances diminish to 14% for a threshold of 12 m and 0.5% for a threshold of 21 m. Exceedance probabilities for July and S2 are naturally much smaller compared to January and demonstrate the added information that can be extracted from our non-stationary model.

Omni-directional TP for January should also be less than omni-directional TP for the omni-seasonal case even though January is one of the months most prone to large waves. As shown in Table 2, indeed, the omni-seasonal/directional TP values (annual values) are again larger than the omni-directional TPs for January or July in Table 1. This makes sense since it is more likely to experience large waves allowing for 12 months to pass compared to only considering a single month. The monthly omni-seasonal probability (CP) denotes the probability for a wave to exceed the threshold given a random month. This again needs to be lower than the probability for January because also a month with lower wave climate might be drawn.

The TPs and CPs from Table 2 and Fig. 9 summarize and compare the results for the omni-seasonal/directional results from our non-stationary model versus an annual block maxima baseline stationary model. Broadly speaking, these results condense what could be seen from the probability landscapes, a wave exceeding 12 m is almost certain to occur every year with an omni-directional/seasonal $\mathrm{TP}(X > 12\,\mathrm{m}) = 0.987$ while exceeding 21 m has an omni-directional/seasonal of $\mathrm{TP}(X > 21\,\mathrm{m}) = 0.057$, which equates to a return period of roughly 17.5 years. The stationary model predicts similar results but yields increasingly higher probabilities the further one moves out into the tail, illustrated for omni-seasonal/directional CPs in Fig. 9 (left). Although the probabilities differ slightly between the stationary model and the non-stationary model, the stationary model is a probable outcome from our non-stationary model and it falls well within the distribution of probabilities from our non-stationary model (Fig. 9 right).

Table 2
Exceedance probabilities for annual block maxima of stationary baseline model and our non-stationary GAM model for the omni-directional/omni-seasonal case. Probabilities are computed for a threshold of 12 m and 21 m based on 1000 model predictions for each considered scenario. Annual scaling for the non-stationary model is derived with the logic from Eq. (10).

	Stationary model OD and OS	Non-stationary OD and OS (monthly)
$P(H_U > 12\,m)$	0.994	0.987 (0.306)
$P(H_U > 21\,m)$	0.091	0.057 (0.005)

5. A brief application to normalized wave heights

The standard approach, i.e., all sea state approach or initial distribution method (IDM), would, in this context, focus on plotting all normalized wave heights (H_{norm}) according to their probability, together with e.g. a 2-parameter Weibull distribution to finally compare against theoretical distributions such as Forristall and Rayleigh (see Fig. B.13 for omni-seasonal and omni-directional estimates). For different sectors and seasons the data is typically split, which reduces the respective amount of information, and results may require arbitrary scaling. Since there are two variables H_U and H_s, at least one needs to be given in order to retrieve a probability. Further assumptions on a representative wave period are needed to transform the number of waves to the time domain, i.e. transform a 1 in 10 000 waves exceedance probability to something like a daily or monthly exceedance probability. Our novel framework provides a probability in a unit time, and if desired direction, without prior knowledge and without having to rely on theoretical distributions that in turn have assumptions on the characteristics of the waves.

Moreover, our approach can just as well be applied to H_{norm} which may be easier to directly adapt to metocean applications. As an example, we briefly explore the behavior of H_{norm} across the covariate space by fitting the same GAM model to the respective H_{norm} (see QQ-plot Fig. C.14). If interested in sectorial or seasonal estimates one can follow the same steps as already described above. Instead of exceedance probability, we display the model's median prediction of H_{norm} depending on season and direction (Fig. 10). Slight variations between 1.86 and 1.96 are evident along season and direction. These variations are nevertheless noteworthy, as H_{norm} effectively is a factor. For H_s of, e.g. 10 m the corresponding maximum individual wave would vary about 1 m depending on season and direction. While the displayed return level landscape may vary from location to location, these results reveal an important underlying message. The assumption of a universally applicable, all sea state theoretical distribution, or a stationary IDM applied to all data may lead to erroneous assumptions on the wave climate and subsequently the design of offshore structures.

6. Discussion and limitations

We created a modeling framework to extract individual seasonal–directional extreme waves and their exceedance probabilities for the Ekofisk complex utilizing novel datasets.

The model and our framework can further be refined and adjusted to common user needs such as conditioning on the sea state. As already mentioned, the monthly maxima are heavily connected to the sea state variable H_s which explains most of the variation and hijacks some of the seasonal and directional information we would like to extract. However, although to a limited extent, we can indirectly condition the model by only allowing maxima above a given sea state threshold (not shown). Another common covariate of interest is the sea level. This variable could be either added to the model (although that might mean to adjust and possibly reduce the number of knots for the spline fits) or exchange one of the covariates.

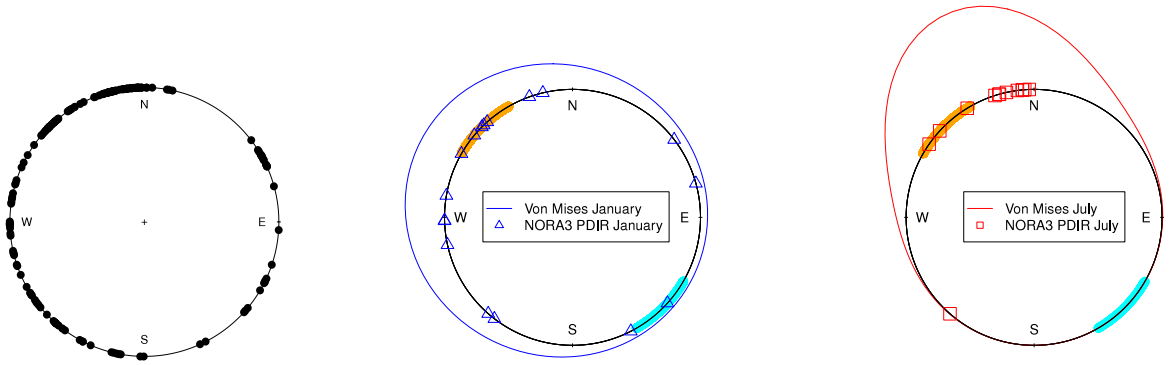

Fig. 8. Left: Empirical distribution of PDIR. Center/Right: Empirical distribution and von Mises density for PDIR of two months (January, July) as well as two directional sectors are displayed, 300–330° (orange) and 120–150° (cyan).

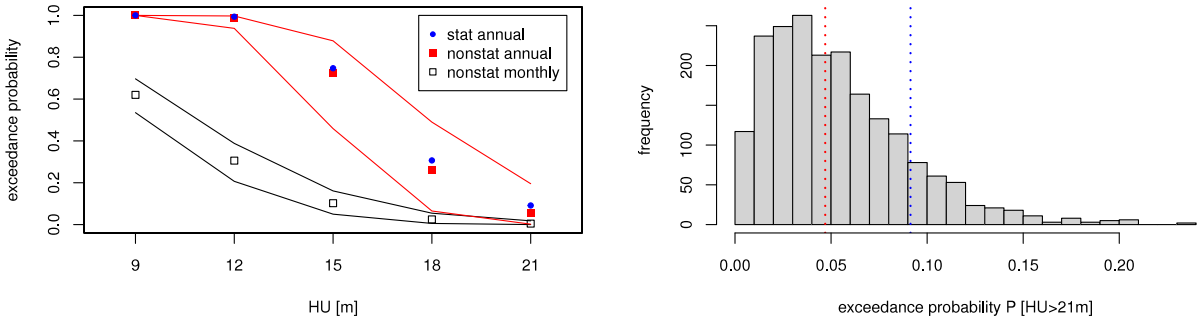

Fig. 9. Left: Comparison of exceedance probabilities (omni-directional/seasonal TP for random month) for various H_U between a stationary model and a seasonal–directional model with prediction intervals based on the estimation of the β's in gray (0.5% and 99.5%). Right: Histogram of distribution of exceedance probabilities (omni-directional/seasonal TP for a random month) for $P[H_U > 21\,\text{m}]$ from our non-stationary GAM model divided into 20 regularly spaced bins. The stationary exceedance probability is displayed as a red stippled line.

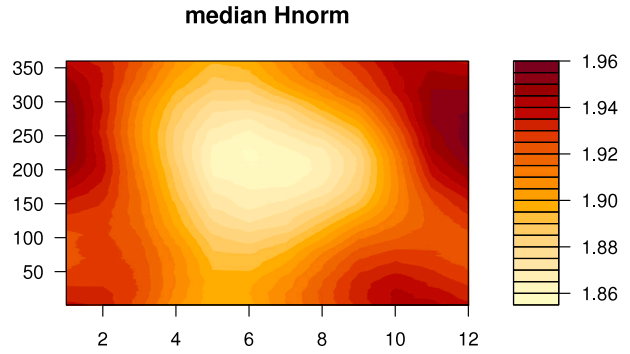

Fig. 10. Prediction of median for H_{norm} along the entire covariate space, i.e. months (1–12) and direction (0–360°).

This framework may also be applied to other met-ocean variables like wind, current, and integrated wave parameters like H_s. Additionally, not only offshore locations but also coastal applications can be considered. However, especially in fjord like geometries, where channeled wind and fetch length may allow for a bi-modal distribution of directions, the cyclic model needs to be revised. Once modeling of occurrences of directions is settled one can continue with the here presented framework.

For the purpose of this study, we consider our approach more intuitive than the artificial scaling described in the offshore standards. Although we involve a more complex model, once established, one only counts exceedances from simulated extremes being the basic empirical approach of calculating exceedance probabilities. Hence, the probabilities are more understandable, interpretable, and ultimately more tangible for the end-user.

Some limitations are important to keep in mind when considering extremes from the here presented non-stationary model. The directions used for the model fit were not measured but are from a numerical model hindcast (NORA3). Although it has been shown that both the quality of the wind forcing (Haakenstad et al., 2021) and of the simulated waves (Breivik et al., 2022) even surpass the state-of-the-art, NORA10 (Reistad et al., 2011), they are merely from a discretized, numerical model. The directions in NORA3 are binned (36 directions encompassing 10 degrees each) but PDIR undergoes a quadratic interpolation prior to model output which makes the directions appear smooth in the figure (Fig. 4 center) in contrast to clearly visible bins in NORA10 directions (not shown). Another limitation is the lack of a censoring mechanism in the model which might impair, although probably only to a minor degree, the return levels and exceedance probabilities during summer. Supported by the performed model checking we cannot observe a mismatch for the low to medium extremes and consider this effect in our case negligible. Additionally, the use of block maxima leads to a comparably small sample size increasing uncertainty connected to the limited number of samples.

A final limitation is connected to an incident in 1 November 2006 when the bridge, where the lasers were mounted, was hit by an individual wave. Unfortunately, only one laser was active and since the bridge was hit, this event was not reliably recorded with the main wave event missing leaving the wave height remain hidden. Not including drastic events like this might yield a negative bias in exceedance probabilities of the highest waves. We tested the sensitivity to such an event by replacing the October 2006 event of about 23 m with a considerably increased value of 27 m. The October 2006 event was chosen for replacement since the missing wave was from the same storm as the October and November events 2006, and should as such not be counted double. While the exceedance probabilities remain similar for the lower waves (not shown), the highest waves exceeding 21 m experience a

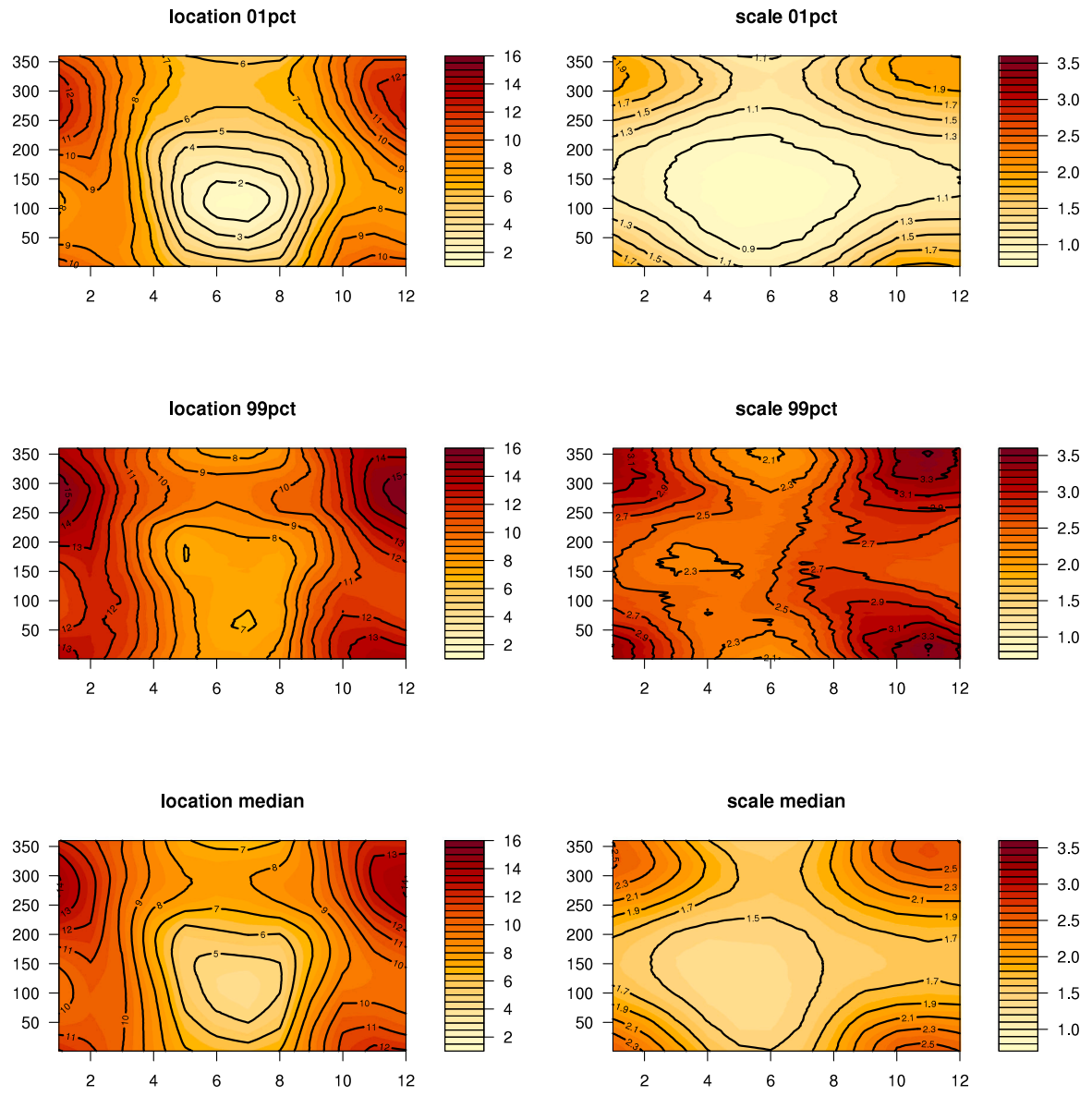

Fig. A.11. Quantiles of location and scale parameters from our non-stationary GAM GEV model for the entire covariate space.

noticeable change from an omni-seasonal/directional TP of 0.057 to ca 0.08 which equates to a return period of about 12.5 years instead of 17.5 years. At this place, it is important to reflect on the uncertainty for exceedance probabilities of such extreme waves. As shown in Fig. 9 (right), a change from 0.057 to 0.08 is still well within the probability range induced by uncertainty on the estimation of the βs in our model. In fact, the valid range allows easily for a much larger change. Having this in mind, we consider the impact of such a missed extreme event tolerable, especially when compared to the uncertainty of our GAM model.

Left or right censoring or arbitrary periods of missing values are a common issue when dealing with observations. There is no easy recipe for dealing with these challenges, especially when the censoring mechanism behind is difficult to quantify, and the alternatives are sparse. Other observation data, e.g. from wave buoys, often come with an inherent low bias especially for the highest and steepest waves due to their hydrodynamic behavior (Allender et al., 1989; Casas-Prat and Holthuijsen, 2010; Barbariol et al., 2019). This is an issue which does not apply to our filtered laser dataset. Using, on the other hand, sea states from a spectral numerical wave model and subsequently generating individual waves using theoretical distributions (as e.g. Rayleigh) is, especially for complex seas with very steep waves, typically biased, as not all physical mechanisms are included. In fact, we show that such a use may yield misleading results as the quantiles of normalized wave heights can vary. For the theoretical distributions the sea states, and often other additional parameters, need to be known which come with additional uncertainty.

All options considered, we believe our approach to provide realistic exceedance probabilities and valuable, additional information of the seasonal and directional variation and magnitude of individual extreme waves.

7. Conclusion and outlook

We have constructed a versatile seasonal–directional, block maxima, extreme value model for Ekofisk primarily based on high frequency laser altimeter measurements of the sea surface and PDIR from the NORA3 hindcast archive. The omni-seasonal/direction exceedance probabilities of monthly maxima are consistent with a stationary GEV model. Compared to a stationary model, our non-stationary model and the presented framework comes with rich and useful information along the covariate space and indicate that at Ekofisk the highest waves are

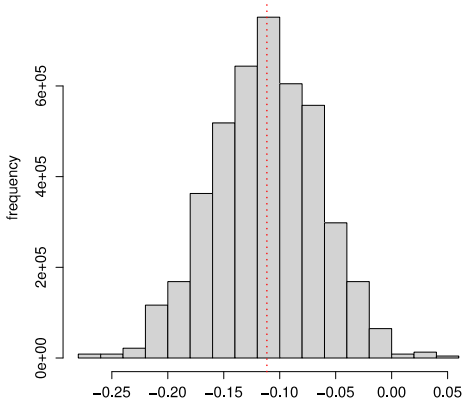

Fig. A.12. Empirical distribution of the shape parameter. Red, stippled line depicts the median.

likely to approach from northwest during winter. We further reveal a non-stationarity in the quantiles of the normalized wave heights with implications for offshore design.

Future work could aim at understanding and modeling the censoring mechanism in the dataset. We are also planning to create a seasonal–directional point process (PP) model to estimate the extremes and in particular investigate normalized wave heights. A better understanding of the censoring mechanism could come in handy for this task. Once the PP model is formulated much of the here described procedure can be repeated to extract the exceedance probabilities. Another interesting continuation would be to extract the directional information from the laser array. This is challenging and we have not yet come to a satisfying result, but in theory this should be possible and could yield exciting and valuable insights.

CRediT authorship contribution statement

Patrik Bohlinger: Conceptualization, Methodology, Analysis, Figures, Code, Writing. **Theodoros Economou:** Conceptualization, Methodology, Code, Writing. **Ole Johan Aarnes:** Methodology, Discussions, Comments, Figure. **Mika Malila:** Discussions, Comments, Figure. **Øyvind Breivik:** Discussions, Comments.

Declaration of competing interest

The authors declare that they have no known competing financial interests or personal relationships that could have appeared to influence the work reported in this paper.

Data availability

The used data is publicly accessible.

Acknowledgments

P.B., O.J.A., M.M., and Ø.B. gratefully acknowledge the funding support from the projects StormRisk (grant no. 300608 from the Research Council of Norway), ConocoPhillips through research for the Extreme Wave Warning service (EXWW) and the Joint Industry Project StereoWave funded by Equinor and ConocoPhillips. T.E. was funded by the European Union's Horizon 2020 research and innovation programme under grant agreement No. 856612 and the Cyprus Government.

Appendix A. Model parameters

See Figs. A.11 and A.12.

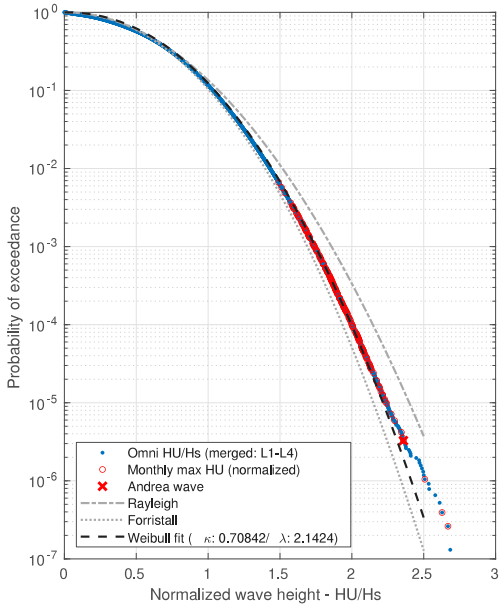

Fig. B.13. Probability of normalized wave height along the theoretical distributions Rayleigh an Forristall and a standard two-parameter Weibull fit. The blue dots depict all waves contained in the dataset with the monthly maxima, used in this study, marked in red. The red cross denotes the Andrea wave.

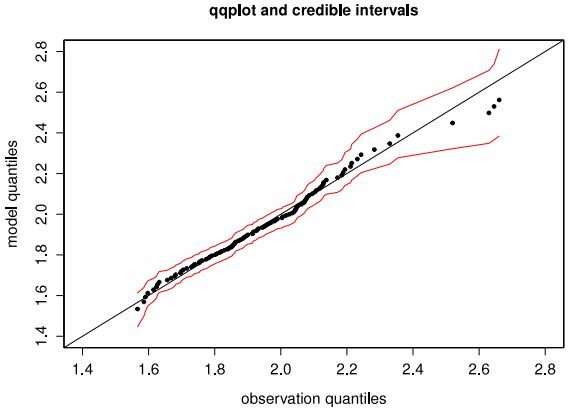

Fig. C.14. A QQ-plot comparing the mean of 1000 simulated values for each observation (black) with 2.5% and 97.5% quantiles as credible intervals (red) against the quantiles from the observations.

Appendix B. Standard approach

See Fig. B.13.

Appendix C. GAM on normalized wave heights

See Fig. C.14.

References

Agostinelli, C., Lund, U., 2022. R package 'circular': Circular statistics (version 0.4-95). URL: https://r-forge.r-project.org/projects/circular/.

Allender, J., Audunson, T., Barstow, S., Bjerken, S., Krogstad, H., Steinbakke, P., Vartdal, L., Borgman, L., Graham, C., 1989. The WADIC project: A comprehensive field evaluation of directional wave instrumentation. Ocean Eng. 16 (5–6), 505–536.

Barbariol, F., Benetazzo, A., Bertotti, L., Cavaleri, L., Durrant, T., McComb, P., Sclavo, M., 2019. Large waves and drifting buoys in the Southern ocean. Ocean Eng. 172, 817–828.

Bell, R.J., Gray, S.L., Jones, O.P., 2017. North Atlantic storm driving of extreme wave heights in the North Sea. J. Geophys. Res.: Oceans 122 (4), 3253–3268.

Bohlinger, P., Breivik, Ø., Economou, T., Müller, M., 2019. A novel approach to computing super observations for probabilistic wave model validation. Ocean Model. 139, 101404.

Breivik, Ø., Carrasco, A., Haakenstad, H., Aarnes, O.J., Behrens, A., Bidlot, J.R., Björkqvist, J.V., Bohlinger, P., Furevik, B.R., Staneva, J., et al., 2022. The impact of a reduced high-wind Charnock parameter on wave growth with application to the North Sea, the Norwegian Sea and the Arctic ocean. J. Geophys. Res.: Oceans e2021JC018196.

Casas-Prat, M., Holthuijsen, L.H., 2010. Short-term statistics of waves observed in deep water. J. Geophys. Res.: Oceans 115 (C9).

Christou, M., Ewans, K., 2014. Field measurements of rogue water waves. J. Phys. Oceanogr. 44 (9), 2317–2335.

Coles, S., 2001. An Introduction To Statistical Modeling of Extreme Values. In: Springer Series in Statistics, Springer-Verlag, London.

Donelan, M.A., Magnusson, A.K., 2017. The making of the Andrea wave and other rogues. Sci. Rep. 7 (44124), http://dx.doi.org/10.1038/srep44124.

Feld, G., Jonathan, P., Randell, D., 2019. On the estimation and application of directional design criteria. In: International Conference on Offshore Mechanics and Arctic Engineering, Volume 7B: Ocean Engineering. http://dx.doi.org/10.1115/OMAE2019-96586.

Feld, G., Randell, D., Wu, Y., Ewans, K., Jonathan, P., 2014. Estimation of storm peak and intra-storm directional-seasonal design conditions in the North Sea. In: International Conference on Offshore Mechanics and Arctic Engineering, Volume 4A: Structures, Safety and Reliability. http://dx.doi.org/10.1115/OMAE2014-23157.

Gelman, A., Carlin, J., Stern, H., Dunson, D., Vehtari, A., Rubin, D., 2013. Bayesian Data Analysis, third ed. Chapman and Hall/CRC, http://dx.doi.org/10.1201/b16018.

Gilleland, E., Katz, R.W., 2016. extRemes 2.0: An extreme value analysis package in R. J. Stat. Softw. 72 (8), 1–39. http://dx.doi.org/10.18637/jss.v072.i08.

Haakenstad, H., Breivik, Ø., Furevik, B., Reistad, M., Bohlinger, P., Aarnes, O.J., 2021. NORA3: A nonhydrostatic high-resolution hindcast of the North Sea, the Norwegian Sea, and the Barents Sea. J. Appl. Meteor. Climatol. 60, 1443–1464. http://dx.doi.org/10.1175/JAMC-D-21-0029.1.

Häfner, D., Gemmrich, J., Jochum, M., 2021. FOWD: A free ocean wave dataset for data mining and machine learning. J. Atmos. Ocean. Technol. 38 (7), 1305–1322.

Hansen, H.F., Randell, D., Zeeberg, A.R., Jonathan, P., 2020. Directional–seasonal extreme value analysis of North Sea storm conditions. Ocean Eng. 195, 106665.

Jonathan, P., Ewans, K., 2011. Modeling the seasonality of extreme waves in the Gulf of Mexico. J. Offshore Mech. Arct. Eng. 133.

Jonathan, P., Ewans, K., 2013. Statistical modelling of extreme ocean environments for marine design: A review. Ocean Eng. 62, 91–109.

Jonathan, P., Ewans, K., Forristall, G., 2008. Statistical estimation of extreme ocean environments: The requirement for modelling directionality and other covariate effects. Ocean Eng. 35 (11–12), 1211–1225.

Malila, M.P., Barbariol, F., Benetazzo, A., Breivik, Ø., Magnusson, A.K., Thomson, J., Ward, B., 2022a. Statistical and dynamical characteristics of extreme wave crests assessed with field measurements from the North Sea. J. Phys. Oceanogr.

Malila, M.P., Bohlinger, P., Støle-Hentschel, S., Breivik, Ø., Hope, G., Magnusson, A.K., 2022b. A nonparametric, data-driven approach to despiking ocean surface wave time series. J. Atmos. Ocean. Technol. 39 (1), 71–90.

NORSOKSTANDARD N-003, 2017. Actions and action effects. Technical Report, NORSOK STANDARD, URL: http://www.standard.no.

Rayleigh, L., 1880. On the resultant of a large number of vibrations of the same pitch and of arbitrary phase. Lond. Edinb. Dublin Philos. Mag. J. Sci. 10 (60), 73–78.

Reistad, M., Breivik, Ø., Haakenstad, H., Aarnes, O., Furevik, B., Bidlot, J.R., 2011. A high-resolution hindcast of wind and waves for the North Sea, the Norwegian Sea, and the Barents Sea. J. Geophys. Res.: Oceans 116 (C5).

Tayfun, M.A., 1980. Narrow-band nonlinear sea waves. J. Geophys. Res.: Oceans 85 (C3), 1548–1552.

von Mises, R., 1918. Über die Ganzzahligkeit der Atomgewichte und verwandte Fragen. Phys. Z. 19, 490–500.

Wood, S.N., 2006. Low-rank scale-invariant tensor product smooths for generalized additive mixed models. Biometrics 62 (4), 1025–1036.

Wood, S.N., 2011. Fast stable restricted maximum likelihood and marginal likelihood estimation of semiparametric generalized linear models. J. R. Stat. Soc. Ser. B 73 (1), 3–36. http://dx.doi.org/10.1111/j.1467-9868.2010.00749.x.

Wood, S.N., 2017. Generalized Additive Models: An Introduction with R, second ed. In: Chapman & Hall/CRC texts in statistical science, Chapman and Hall/CRC.